Theoretical Study of Ductile Fracture in Steel Structures in the Presence of Spatial Variability in Toughness

Vincente Pericoli, S.M.ASCE¹; and Amit Kanvinde, M.ASCE²

Abstract: Micromechanical or local models are increasingly used for predicting microvoid-growth-induced ductile fracture in structural steel components. Methods to calibrate and apply these models presume that both calibration specimens and prototypical components are spatially homogenous in terms of material toughness. This presumption conflicts with test data that show significant variability in material toughness of coupons extracted from a larger steel sample. Spatial variability of toughness in structural components has the potential to diminish deformation capacity due to the statistical size effect, which arises from weakest-link sampling. To examine this issue, two material representations are evaluated against a set of 32 experiments on two types of structural steel, using a maximum likelihood estimation-based approach. One approach represents the material as homogenous with random toughness (as implicitly assumed by prevailing methods), whereas the other represents the material as heterogeneous with spatially random toughness. No significant difference is observed between the two approaches in predicting test data. This suggests that the material is approximately homogenous over the sizes of the tested coupons, with spatial variability present only over larger length scales. To examine the potential effects of such variability, parametric finite-element studies are conducted on a prototypical fracture-critical detail. The results confirm the statistical size effect, such that larger details have lower deformation capacity. Current methods are not able to capture this effect when transferring fracture toughness from lab-scale to archetype-scale components. A parameter is proposed to facilitate this type of scaling. DOI: 10.1061/(ASCE)ST.1943-541X.0002008.

Author keywords: Fracture; Steel structures; Spatial randomness.

Introduction

Over the last three decades, beginning with the 1994 Northridge and 1995 Kobe earthquakes, approaches to predict steel fracture in civil structures have made significant progress. Linear-elastic fracture mechanics or elastic-plastic fracture mechanics are adequate to assess brittle fractures similar to those observed in the 1994 Northridge Earthquake (Chi et al. 2000). Other situations, e.g., post-Northridge steel connections as outlined in FEMA (2000), that may not have a pre-existing crack or that involve largescale yielding prior to fracture, invalidate the assumptions of linearelastic or elastic-plastic fracture mechanics (Anderson 1995). Micromechanics-based or local fracture models overcome these limitations, and major advances have been made in their development and application (Besson et al. 2006), with the result that they are increasingly used by the research and engineering communities (Kiran and Khandelwal 2013; Amiri et al. 2013; Kanvinde 2017). In contrast to far-field parameters such as the stress intensity factor K_I or the J-integral J_I , local criteria are expressed as critical combinations of continuum strains and stresses. The functional forms of these criteria reflect micromechanisms such as microvoid growth and coalescence (Rice and Tracey 1969) associated with ductile fracture, or granular cleavage (Ritchie et al. 1973) associated with brittle fracture. Adaptations of these models to civil structures address shear-dominated stress states (Wen and Mahmoud 2016; Smith et al. 2014) and earthquake-induced cyclic loading (Kanvinde and Deierlein 2007). This paper focuses on local models used to predict ductile crack initiation due to microvoid growth and coalescence, e.g., the void growth model of Hancock and Mackenzie (1976). Prediction of ductile crack initiation is critical from the standpoint of structural performance assessment because it is usually the precursor to brittle propagation in steel components without sharp cracks.

Mechanistic aspects of local models for ductile fracture are mature, meaning that the underlying micromechanisms are wellunderstood, and the associated functional forms have been extensively validated (Kanvinde 2017). However, other aspects of these models are not so well-developed. For example, it is nominally assumed (with the exception of weld regions) that structural components are spatially homogenous in terms of material toughness (Prinz and Richards 2015; Khandelwal and El-Tawil 2007). Although this assumption may be justified for coupon-scale (~50 mm) laboratory tests or components in which a small region of the material is strained, its extension to prototype-scale components (>500 mm) is questionable. This is because larger components subject a greater volume of material to high strains, leading to a higher probability of sampling weak links in the material microstructure, ultimately diminishing deformation capacity. Statistical size-effects are well-documented in the literature for both steel (Weibull 1939) and concrete (Bažant 2005), indicating that the assumption of spatial homogeneity results in nonconservative estimates of fracture. Although this is concerning in itself, closer scrutiny reveals additional problems

1. The notion of spatial homogeneity conflicts with material calibration data sets, which routinely suggest significant variability (coefficient of variation on the order of 15–22%) in

¹Graduate Research Assistant, Dept. of Civil and Environmental Engineering, Univ. of California, Davis, CA 95616.

²Professor, Dept. of Civil and Environmental Engineering, Univ. of California, Davis, CA 95616 (corresponding author). E-mail: kanvinde@ucdavis.edu

Note. This manuscript was submitted on April 26, 2017; approved on October 18, 2017; published online on February 16, 2018. Discussion period open until July 16, 2018; separate discussions must be submitted for individual papers. This paper is part of the *Journal of Structural Engineering*, © ASCE, ISSN 0733-9445.

material toughness parameters (Kanvinde and Deierlein 2006; Liao et al. 2012). Because these calibration specimens (~10–50 mm) are usually extracted from a larger (>500 mm) parent sample of steel (e.g., a rolled plate or section), the variability among them confirms that the parent sample is internally heterogeneous.

- Local models require resolution of stress and strain fields over length scales on the order of steel grain size (~0.1 mm). The notion of material homogeneity is not well-supported at this scale due to heterogeneities in crystal structure and irregularly distributed inclusions (de Geus et al. 2015; Jeulin and Ostoja-Starzewski 2001).
- 3. Experimental data (e.g., Myers et al. 2010; Hazarabedian et al. 2002) also support the weakest-link hypothesis. Specifically, larger components exhibit lower unit resistance to fracture and also show lower variability in fracture strength or deformation, because fracture is controlled by extreme (lower) values of material toughness. This is consistent with extreme value theory (Bažant et al. 2004). Methods that presume the material to be homogenous cannot reproduce these trends, impeding the extrapolation of lab-scale calibration tests to larger structural components.

These issues are also problematic when viewed against current trends in structural performance assessment that emphasize accurate characterization of extreme limit states in a probabilistic framework (FEMA 2009). Motivated by these issues, this paper critically examines (1) alternative methodologies to represent spatial variation in material toughness as it pertains to ductile initiation, (2) implications of disregarding spatial variation, and (3) strategies to mitigate scaling effects in the presence of this variability. The paper begins by providing background with respect to previous work in this area. This is followed by a discussion of an experimental program conducted by Kanvinde and Deierlein (2004). These tests are used as a test bed for examining alternative representations of spatial variations in material toughness, which are discussed in a subsequent section. Finally, parametric finite-element (FE) simulations are presented to examine the effects of spatial variability on fracture in a prototypical detail.

Background

This section summarizes research on ductile fracture in structural steel as it pertains to this study, including (1) an established local model for ductile fracture and (2) previously developed approaches for considering spatial randomness in the context of brittle as well as ductile fracture.

Void Growth Model for Predicting Ductile Fracture in Structural Steel

The void growth model (VGM) (McClintock 1968; Rice and Tracey 1969) is an extensively verified (Chen and Butler 2013; Panontin and Sheppard 1995) criterion to simulate ductile fracture that initiates through the processes of microvoid growth and coalescence (Fig. 1). The VGM criterion is

$$\int_{0}^{\varepsilon_{p}^{fracture}} \exp(1.5 \times T) \cdot d\varepsilon_{p} = \eta \ge \eta_{cr} \quad \text{over any } r \ge l^{*}$$
 (1)

where η = indicator of microvoid growth, and represents damage at any continuum location; and η_{cr} = critical value of η , and may be interpreted as a material capacity or resistance to ductile fracture, calibrated through coupon testing (Myers et al. 2010), whereas η is the counterpart demand, determined by integrating stress and strain quantities (i.e., the triaxiality $T = \sigma_m/\sigma_e$ and the equivalent plastic strain ε_p) usually obtained from FE simulations of the component of interest. To ensure sufficient sampling of microstructural features, ductile fracture is predicted at any location when the criterion described by Eq. (1) is satisfied at all locations over any line segment of l^* originating at that location (Panontin and Sheppard 1995; Chi et al. 2006). Thus the VGM is defined by two parameters, η_{cr} and l^* . The criterion in Eq. (1) and the associated sampling check may be expressed more conveniently in mathematical form as

$$\eta_{reg} \ge \eta_{cr}$$
 (2)

where

$$\eta_{reg}(\mathbf{x}) = \max_{\theta} (\min(\eta[\mathbf{x}, \mathbf{x} + l^*]_{\theta}))$$
 (3)

where η = demand at any location \mathbf{x} [determined from Eq. (1)]; $\min(\eta[\mathbf{x},\mathbf{x}+l^*]_{\theta})=\min$ minimum value of η over a line segment of length l^* originating at \mathbf{x} ; and θ = arbitrary direction in space, such that the regularized value of η , i.e., η_{reg} , is the maximum of such minima over segments radiating in all directions from \mathbf{x} . Once transformed in this manner, a pointwise check applied to the regularized η_{reg} field results in predictions of fracture identical to those based on Eq. (1) followed by the explicit sampling check over the neighborhood. This means that the fracture criterion may be expressed more conveniently as

$$\eta_{reg}^{\text{max}} \ge \eta_{cr}$$
(4)

where η_{reg}^{max} = maximum value of η_{reg} over the entire volume of the specimen or component. Formulation of the VGM in this manner is crucial for this study, which heavily relies on pointwise evaluations of the fracture criterion to analyze the influence of spatial

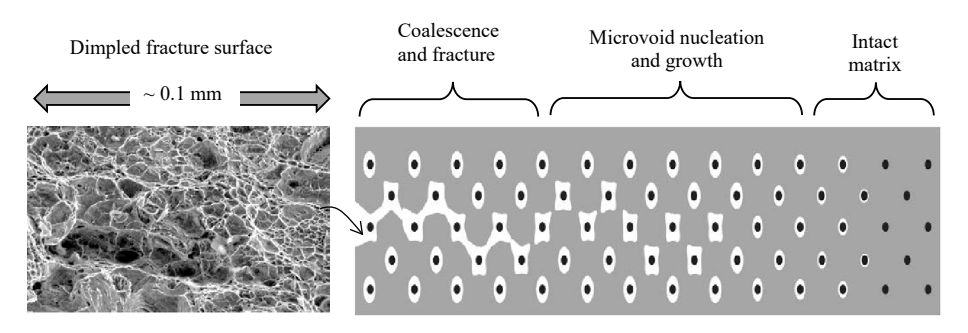


Fig. 1. Microvoid nucleation, growth, and coalescence leading to dimpled surface characteristic of ductile fracture in low-carbon structural steel

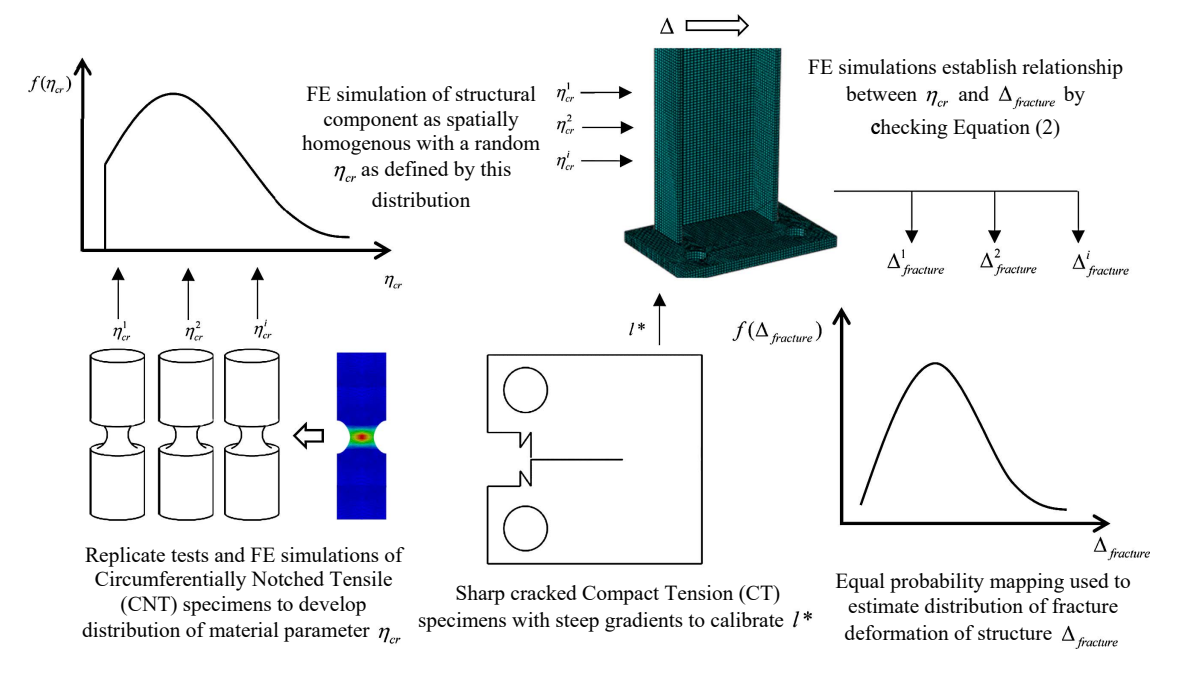


Fig. 2. Schematic illustration of prevalent methodology for predicting fracture in steel components using local models

randomness. Nonregularized stresses (which are unbounded in the vicinity of sharp flaws) invalidate these evaluations. Accordingly, the approach presented in this paper, and subsequent references to the VGM, are based on the regularized interpretation and pointwise evaluations (e.g., η generically refers to η_{reg}). Fig. 2 schematically illustrates the methodology for predicting ductile fracture initiation using the VGM (or similar models). The main elements of this methodology are (1) calibration of the toughness parameter η_{cr} and length scale l^* using coupon tests; circumferentially notched tensile (CNT) specimens have flat gradients unaffected by l^* , and are used to isolate and calibrate η_{cr} (and its statistical distribution, through replicate tests), and sharp cracked geometries with steep gradients, such as compact tension (CT) specimens, enable effective calibration of l^* once η_{cr} has been calibrated; (2) simulation of stress triaxiality and plastic strain fields, usually using FE simulation; and (3) evaluation of the VGM criterion, i.e., Eq. (4), to determine fracture initiation. This methodology implicitly presumes that the material is spatially homogenous, i.e., η_{cr} is constant throughout the component. This is inconsistent with experimental data that indicate variability over larger material samples.

Previous Research to Incorporate Spatial Randomness into Fracture Prediction in Steel

The Weibull stress approach (Beremin 1983) reflects weakestlink processes that trigger stress-controlled cleavage fracture, by expressing the fracture criterion in a probabilistic manner

$$P_f = 1 - \exp[-(\sigma_w/\sigma_u)^m] \tag{5}$$

where

$$\sigma_w = \left[(1/V_0) \int_{\Omega} \sigma_{peak}^m \cdot dV \right]^{1/m} \tag{6}$$

 σ_w = demand quantity determined as a volume averaged peak (i.e., maximum principal tensile) stress over the entire component volume Ω , and when calculated in this manner, σ_w corresponds to a consistent probability of failure, considering weakest-link

sampling; σ_u and m = model parameters, referred to as Weibull moduli; and V_0 = arbitrary reference volume, selected in conjunction with the Weibull moduli. Beremin (1983) outlined theoretical underpinnings of this approach, and Matos and Dodds (2001) and Lambert-Perlade et al. (2004) summarized refinements and applications to structural engineering problems (beam-column connections and welded connections).

Pineau and Joly (1991) incorporated weakest-link processes in ductile fracture by establishing relationships between distributions of a critical void ratio and the critical J-integral J_{IC} . Devillers-Guerville et al. (1997) conducted a process similar to that shown in Fig. 2, with the exception that the coupons and the structural component were divided into a grid of regions, each with its own material toughness [represented as void porosity within a Gurson (1977) model], sampled from a predetermined distribution. Becker (1987) conducted similar simulations. These studies indicated that spatially distributed material properties decrease deformation capacity, due to weakest-link-controlled localization. However, the cited research (informed by small-scale coupons) assumed the material to be spatially stationary (i.e., porosities for all regions in the grid are independently, and identically distributed), an assumption that is not validated. Additionally, those studies used graphical measurements of porosities in the material, which is somewhat constraining because (1) the relatively small volumes of materials (~1 cm) sampled in the measurements may not be representative of larger volumes of material sampled in structural components; and (2) toughness parameters such as η_{cr} , which is back-calibrated from mechanical tests) are more indicative of physical response than are porosities inferred from graphical measurements. Furthermore, the length scales associated with the sampling (analogous to the volume V_0 in the Weibull stress approach) were not explicitly identified, potentially leading to mesh-dependence as different grid sizes are used for material toughness simulation. Myers et al. (2009) addressed the issue of spatial variability in steel fracture for base plate connections by considering a finite number of discrete candidate locations for fracture, recognizing the potential for variability between these. However, their approach did not explicitly consider the spatially continuous variation of properties.

	Specimen type		Number of replicates	Stress triax at fracture	Displacement at fracture, Δ_f (mm)		Maximum η at fracture ^b	
Steel type		Dimensions ^a (mm)			Mean	Coefficient of variation	Mean	Coefficient of variation
A572	CNT	$D_o = 12.7; D_i = 6.35; R_N = 1.524$	2	1.33	0.58	0.06	0.94	0.12
	CNT	$D_o = 12.7; D_i = 6.35; R_N = 3.175$	3	1.12	0.95	0.10	1.52	0.18
	CNT	$D_o = 12.7; D_i = 6.35; R_N = 6.35$	2	0.94	1.26	0.02	1.37	0.03
	CT	W = 50.8; $a/W = 0.5$	2	2.14	0.77	0.16	1.56 ^c	0.33^{c}
	BN	W = 50.8; $a/W = 0.5$; $R = 0.79375$	3	0.60	2.08	0.06	1.13 ^c	0.06^{c}
	RS	$W = 50.8$; $L_G = 76.2$; $t_N = 9.5$; $R_N = 19.0$	2	0.87	6.29	0.01	2.27	0.01
	BH	$W = 50.8$; $L_G = 76.2$; $t_N = 9.5$; $D_B = 12.7$	2	0.68	3.51	0.02	1.90	0.05
	BB	$W = 50.8$; $L_G = 76.2$; $t_N = 9.5$; $D_B = 12.7$	2	0.68	3.40	0.12	1.84	0.24
HPS70W	CNT	$D_o = 12.7; D_i = 6.35; R_N = 1.524$	2	1.51	0.84	0.03	3.46	0.04
	CNT	$D_o = 12.7$; $D_i = 6.35$; $R_N = 3.175$	2	1.24	1.54	0.13	4.67	0.22
	CT	W = 50.8; $a/W = 0.5$	2	2.12	0.91	0.11	3.82^{c}	0.26^{c}
	BN	W = 50.8; $a/W = 0.5$; $R = 0.79375$	2	0.70	8.20	0.09	3.63^{c}	0.08^{c}
	RS	$W = 50.8$; $L_G = 76.2$; $t_N = 9.5$; $R_N = 12.7$	2	1.06	5.41	0.05	3.74	0.16
	BH	$W = 50.8$; $L_G = 76.2$; $t_N = 9.5$; $D_B = 12.7$	2	0.90	3.78	0.05	3.25	0.12
	BB	$W = 50.8$; $L_G = 76.2$; $t_N = 9.5$; $D_B = 12.7$	2	0.89	4.09	0.03	3.51	0.05

^aDimensional quantities in Fig. 3.

Other relevant research on metals (albeit in a nonstructural engineering context) includes work by Ponson et al. (2013), de Geus et al. (2015), and Paquet and Ghosh (2011). Outside of ductile fracture in steel, consideration of spatial randomness is more common; e.g., Andrade et al. (2008) studied the stability of granular media and Feng et al. (2011) studied the properties of laminated composites.

Experimental Data Set and Complementary Finite-Element Simulations

Table 1 summarizes the experimental data set comprising 32 experiments [based on Kanvinde and Deierlein (2004)] used in this study. These experiments encompassed two varieties of low-carbon structural steel, an A572 plate steel with a nominal yield stress of 345 MPa and a high-performance bridge steel (HPS70W) with a nominal yield stress of 485 MPa. Table 2 indicates material-specific data for these steels. Fig. 3 shows the specimen geometries tested—each provides a different level of stress triaxiality, which can be further controlled with parametric variations (e.g., notch size) within specimen types. The circumferentially notched tensile specimens are effective for calibrating the toughness parameter (η_{cr}) of the VGM and other local models because the stress-strain gradients in the CNT specimens (in the region of fracture, i.e., at the center of the notch) are fairly flat, such that the toughness parameter η_{cr} may be calibrated independently from the length scale l^* , which is

Table 2. Material Properties for the Two Steels Used in the Study

	Yield stress (MPa)	Ultimate stress (MPa)	Ductility, d_0/d_f^a	Average grain diameter	Chemical composition (% by weight)	
Steel				(mm)	Carbon	Sulfur
A572 HPS70W	345 552	586 690	1.50 1.95	0.0189 0.0067	0.22 0.08	0.015 0.006

^aRatio of initial:fracture diameter of tension coupon.

engaged in specimens with steeper stress-strain gradients. The blunt-notched (BN) and the compact-tension specimens produced steeper gradients in the vicinity of the notch or crack, enabling material sampling over small (~0.2 mm³) volumes (because the zone of high-strain is fairly concentrated at the crack tip) and effective calibration of l^* . The reduced-section pull plates and the specimens with holes—i.e., reduced-section (RS), bolt-hole (BH), and bolt-bearing (BB) specimens—represent conditions similar to those in smooth structural specimens (e.g., reduced beam sections and bolted connections) and sample a larger volume of material relative to the other specimens. Specimens with higher gradients also enable meaningful examination of the interactions of stressgradients with material heterogeneity. Collectively, the considered tests interrogated a range of stress states, stress-strain gradients, and sampling volumes. Replicate specimens were tested for each parameter set, providing information about randomness.

Table 1 also summarizes the deformation recorded to identify the instant of fracture. This deformation was measured over an appropriate gauge length or between two locations on the specimen (Fig. 3). For the CT specimens, the deformation corresponded to attainment of the J_{IC} value determined in accordance with ASTM E1820 (ASTM 2013), in which crack initiation is estimated through a check of unloading compliance. For the other specimens, the initiation of fracture was identified either by a sudden change in slope of the load-deformation curve or through visual examination. Fig. 4(a) shows a representative load-deformation curve for a CNT specimen, in which ductile fracture is detected through a sudden change in slope, whereas Fig. 4(b) shows a BN specimen in which ductile fracture is detected visually because the load deformation curve does not show a discernible change at the point of fracture. For each experiment, the fracture deformation is denoted $\Delta_{fracture,test}^{i,j}$, where index i corresponds to test number and index j denotes steel type.

Continuum FE simulations were conducted to complement each of the experiments (Fig. 5). Constitutive response (with a von Mises yield surface) was represented as a combination of kinematic hardening through the Armstrong and Frederick (1966) model, and isotropic hardening was represented through an exponential rule.

^bSpatially maximum over the entire component.

^cIn high-gradient tests, the maximum η [regularized according to Eq. (3)] is a function of the l^* .

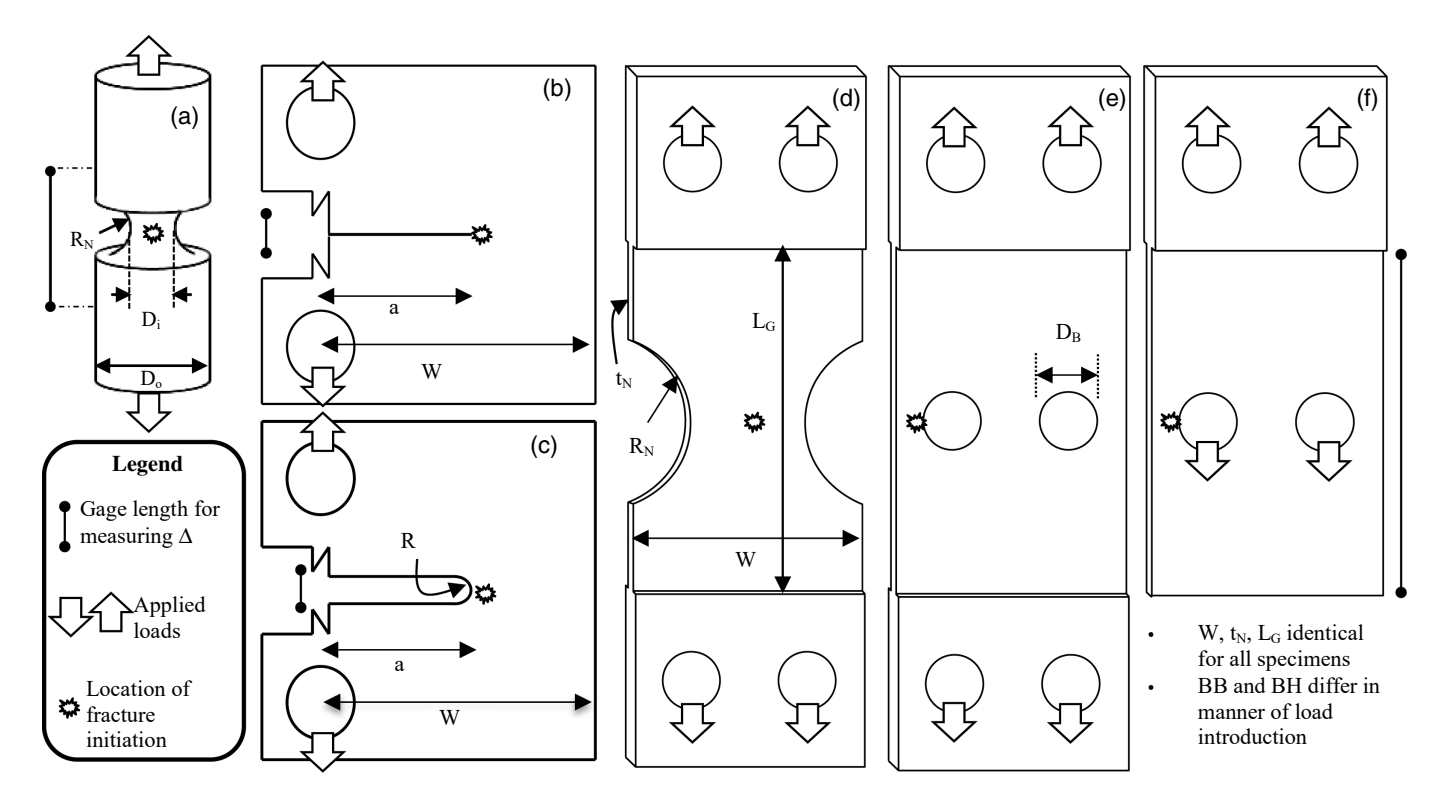


Fig. 3. Specimen geometries: (a) circumferentially notched tensile; (b) compact tension; (c) blunt notched; (d) reduced section; (e) bolt holes; (f) bolt bearing

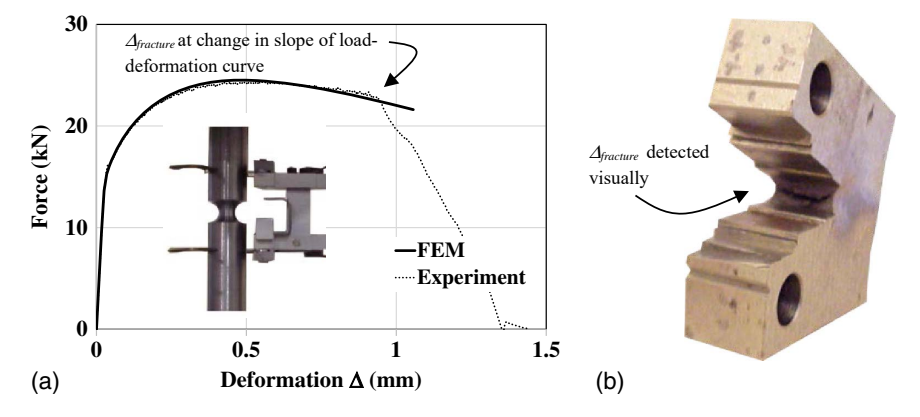


Fig. 4. Detection of ductile fracture through (a) change in load-deformation curve, e.g., for CNT; (b) visual observation, e.g., for BN

For each steel type, constitutive model parameters were calibrated through an automated process developed by Smith et al. (2017) to produce high-quality fits between the load deformation response of FE simulations and the corresponding tests; Fig. 4 shows a representative load-deformation response from FE simulations. Axisymmetric elements (eight-node reduced integration) were used to model the CNT specimens, whereas plane-strain elements (eight-node reduced integration) were used to model the CT specimens. In the BN, RS, BB, and BH geometries, out-of-plane bulging and necking necessitated the use of three-dimensional elements (20-node reduced integration). For each of the models, mesh-sensitivity studies were used to ensure that stress and strain gradients were simulated accurately. The number of elements in the models ranged from 1,500 in the models for the CNT specimens to 52,000 in the models for the BN specimens.

All models were loaded in a manner similar to the corresponding experiments, and the stress-strain field was computed at all spatial locations at each instant of loading. The axisymmetric (for CNT specimens) and plane-strain models (for the CT specimens) achieved computational efficiency by collapsing a dimension (angular for the axisymmetric model and out-of-plane for the plane-strain model), recognizing that the stress-strain fields are constant over the collapsed dimension. These collapsed dimensions cannot represent physical material locations which contribute to the probability of weakest-link fracture. As a result, they are not appropriate for volume sampling. Accordingly, the angular and out-of-plane dimensions were regenerated by replicating the stress-strain field at these locations as determined from the FE simulations. This resulted in proxy models in which the η -field is available at all locations in a three-dimensional sense. A similar process was

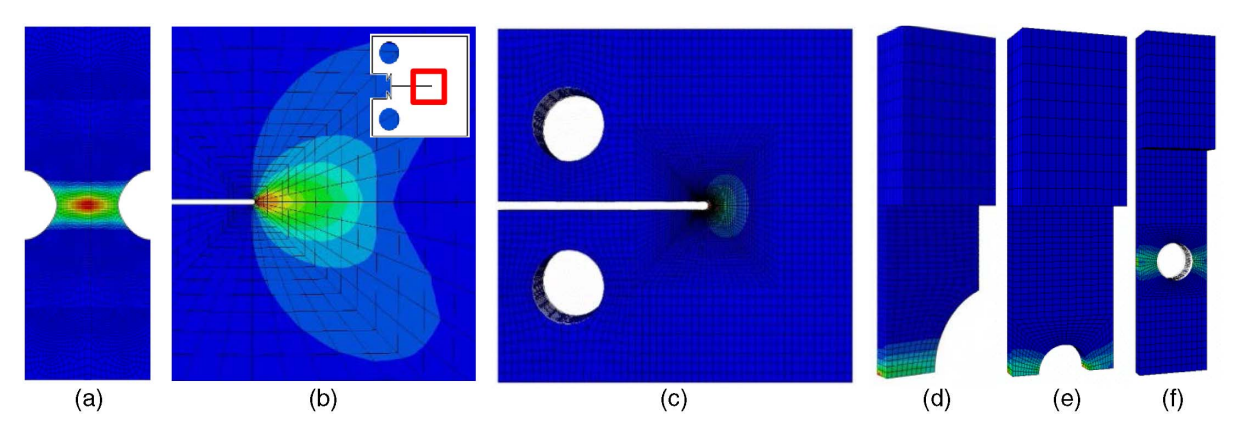


Fig. 5. Finite-element models showing contours of h for (a) CNT—axisymmetric; (b) CT—plane strain, only crack tip mesh shown; (c) BN—3D, $\frac{1}{2}$ model with one plane of symmetry; (d) RS—1/8th model with three planes of symmetry; (e) BH—1/8th model with three planes of symmetry; (f) BB—1/4th model with two planes of symmetry

conducted for the three-dimensional simulations (i.e., for the BN, RS, BB, and BH geometries) because they were simulated with symmetry considerations for computational efficiency (Fig. 5). For these, proxies were developed by regenerating physical locations across planes of symmetry to represent the full material volume. Once the stress-strain fields (for each loading instant at each material location within the proxies) are established in this manner, the instant of fracture may be predicted when the critical condition [Eq. (4)] is satisfied at any location in the model. Evaluation of this condition requires calibration of material parameters (i.e., η_{cr} and l^*) as well as an appropriate representation of the spatial variability in the material toughness η_{cr} , which must be prescribed at all locations. The next section discusses two alternative representations of spatial variability.

Methodologies to Represent Spatial Variation in Fracture Toughness

Once the FE models (or their proxies) are developed as outlined in the preceding section, representations of spatial variability in η_{cr} (hereafter generically referred to as material toughness) may be attached to them; this section considers two alternative representations. One is the homogenous representation, which represents the prevailing methodology, whereas the other considers spatial variability in a manner analogous to the Weibull stress method, albeit in the context of ductile fracture.

Homogenous Random Material

The homogenous random (HR) material method represents the conventional assumption usually implicit in simulating structural components using local models (Fig. 2), such that η_{cr} and l^* are constant over the entire component. Variation is noted in deformation capacity for even nominally identical specimens (Table 1). To explain this, the HR representation implicitly posits that although the specimens themselves are internally homogenous (each with a constant η_{cr}), η_{cr} itself is a random quantity. This may be interpreted to mean that the specimens are sampled from a population of homogenous materials with random toughness (denoted η_{cr}^{HR} to indicate that it represents the toughness of the HR material). Clearly this is not true, because all the specimens were extracted from larger samples (e.g., rolled plates or beams) rather than a population of homogenous materials. A more liberal interpretation is that the specimens are homogenous over their own respective volumes,

even if they are sampled from a larger, spatially heterogeneous plate or beam. In either case, representation of the material in this manner (i.e., homogenous but random) is accomplished by defining the statistical distribution for η_{cr}^{HR} , whereas l^* (which itself is a sampling length scale) is assumed to be deterministic. Based on Myers et al. (2014), a truncated normal distribution was selected to represent randomness in η_{cr}^{HR} . This distribution (Fig. 6) is defined

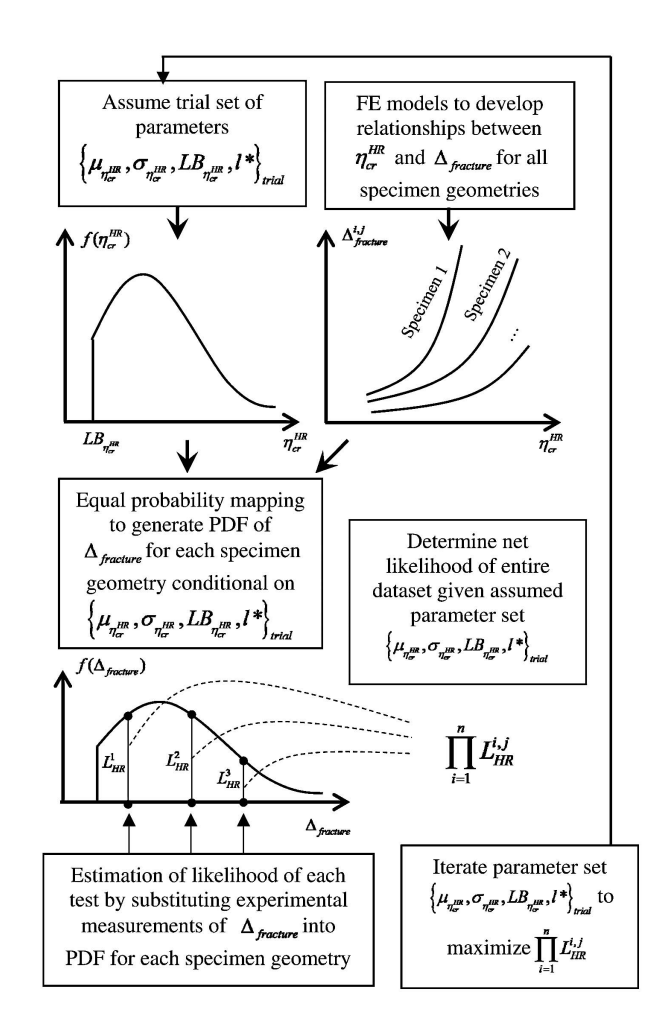


Fig. 6. Schematic illustration of calibration process for HR material representation

by three parameters: the mean and standard deviation $\mu_{\eta^{HR}_{cr}}$, $\sigma_{\eta^{HR}_{cr}}$, and the lower bound value $LB_{\eta^{HR}_{cr}}$. Including l^* , the HR material representation was thus defined by four material parameters. Maximum likelihood estimation (MLE) was used to calibrate these parameters. Myers et al. (2014) provided details of this process as they pertain to calibrating material toughness (Fig. 6); a brief summary of the steps is as follows:

- 1. A trial set of the material parameters $\left\{\mu_{\eta_{cr}^{HR}}, \sigma_{\eta_{cr}^{HR}}, LB_{\eta_{cr}^{HR}}, l^*\right\}_{trial}$ is selected.
- 2. Using the first three (i.e., $\mu_{\eta_{cr}^{HR}}$, $\sigma_{\eta_{cr}^{HR}}$, $LB_{\eta_{cr}^{HR}}$), a trial probability distribution function (PDF) is generated for η_{cr}^{HR} .
- 3. For each FE model (corresponding to a test specimen, defined by the indexes i and j, corresponding to the specimen number and steel type, respectively), a relationship is established between η_{cr}^{HR} and the failure deformation $\Delta_{fracture,FEM}^{i,j}$. This is done by examining the greatest value of η at any location in the proxy model for a given deformation and setting it equal to η_{cr}^{HR} , then recording the corresponding failure deformation. In all cases, this relationship is monotonic (i.e., $\Delta_{fracture,FEM}^{i,j}$ increases with η_{cr}^{HR}).
- 4. Using this relationship and equal probability mapping (Benjamin and Cornell 2014), the PDF of η_{cr}^{HR} is transformed to the PDF $f_{HR}^{i,j}(\Delta_{fracture}^{i,j})$ of the failure deformation $\Delta_{fracture,FEM}^{i,j}$. This PDF is conditional on the trial material parameters $\{\mu_{\eta_{cr}^{HR}}, \sigma_{\eta_{cr}^{HR}}, LB_{\eta_{cr}^{HR}}, l^*\}_{trial}$.
- 5. The PDF generated in this manner may be used in conjunction with experimental data to estimate the likelihood of observing the experimental response of the specimen *i*, *j*, given the assumed set of parameters using the following relationship:

$$L_{HR}^{i,j} = f_{HR}^{i,j}(\Delta_{fracture,test}^{i,j}) \tag{7}$$

This equation inserts the experimental observation of fracture $\Delta^{i,j}_{fracture, \text{test}}$ into the PDF generated using the FE simulation and the assumed set of parameters.

6. Furthermore, the likelihood of observing the entire data set for the particular material (defined by the index *j*) may be calculated as the product of the likelihoods of observing the experimental response of each of the specimens

$$L^{j}(\{\mu_{\eta_{cr}^{HR}}, \sigma_{\eta_{cr}^{HR}}, LB_{\eta_{cr}^{HR}}, l^{*}\}_{trial}) = \prod_{i=1}^{n} L_{HR}^{i,j}$$
 (8)

The likelihood calculated in this manner represents a notional rather than an actual (Hoel 1962) probability of observing the experimental data set given the trial set of parameters $\{\mu_{\eta_{cr}^{HR}}, C_{\eta_{cr}^{HR}}, L_{\eta_{cr}^{HR}}, l^*\}_{trial}$ for material j. A search algorithm is used to determine the optimal set of parameters that maximizes the likelihood $L^j(\{\mu_{\eta_{cr}^{HR}}, \sigma_{\eta_{cr}^{HR}}, L_{\eta_{cr}^{HR}}, l^*\}_{trial})$; this is retained as the calibrated set of material parameters for a given material. Table 3 summarizes the parameters $\{\mu_{\eta_{cr}^{HR}}, \sigma_{\eta_{cr}^{HR}}, L_{\eta_{cr}^{HR}}, l^*\}_{optimal}$ calibrated

Table 3. Calibrated Model Parameters for HR and SR Material Representations

	Fracture model parameters (calibrated using MLE)						
Steel	Model	$\mu_{\eta_{cr}}$	$\sigma_{\eta_{cr}}$	$LB_{\eta_{cr}}$	m	l* (mm)	L^{j}
A572	HR SR	1.340 1.340	0.58 0.58	0.854 0.854	N/A ∞	0.344 0.344	$3.6 \times 10^{22} \\ 3.6 \times 10^{22}$
HPS-70W	HR SR	0.082 0.082	1.77 1.77	2.98 2.98	n/a ∞	0.169 0.169	$1.3 \times 10^{18} \\ 1.3 \times 10^{18}$

in this way for both steels in Table 1. The use of MLE to calibrate the parameters offers advantages over moment fitting, in which sample means, standard deviations (and higher moments) are used to define probability distributions. In addition to robustness and efficiency (Hampel et al. 1986), MLE also provides a way to quantitatively assess the relative likelihood of different methodologies or material representations. More specifically, the likelihoods for each steel variety corresponding to the optimal parameter sets may be multiplied together, to determine L_{HR}^{total} as

$$L_{HR}^{total} = \prod_{j=1}^{n=2} L^{j}(\{\mu_{\eta_{cr}^{HR}}, \sigma_{\eta_{cr}^{HR}}, LB_{\eta_{cr}^{HR}}, l^{*}\}_{optimal})$$
(9)

where L_{HR}^{total} = likelihood of the entire approach (i.e., the HR representation of the material, choice of probability distribution functions, and calibrated parameters) being true. This likelihood may then be compared with counterpart values calculated for alternative methodologies for relative assessment. For the HR material representation, $L_{HR}^{total} = 4.7 \times 10^{40}$. This value is meaningful only in a relative sense, when compared with its counterpart value for the alternate hypothesis, which is discussed next.

Stationary Random Material

Unlike the HR material discussed above, the stationary random (SR) material representation is able to simulate weakest-link sampling by representing the material toughness η_{cr} as spatially random but stationary, meaning that the probability distribution of η_{cr} at all locations is identical and independent of nearby values of η_{cr} . For this purpose, the Weibull stress approach (outlined previously for brittle cleavage) is adapted to ductile fracture initiation. First, the demand quantity σ_{peak} (the peak principal stress for brittle fracture) is replaced with η , and its counterpart capacity σ_u is replaced by η_{cr}^{SR} (the superscript denotes the SR representation). Second, a threshold term η_{th} is introduced to recognize a lowerbound to the material toughness. As pointed out by Gao et al. (1998) and Matos and Dodds (2001), the absence of a threshold admits the possibility of the weakest links having zero (or negligible) toughness. However, because the weakest links control failure probabilities of the entire specimen or component, this results in unrealistic simulation of response. Specifying a positive threshold value of the capacity parameter alleviates this problem. Eqs. (10) and (11) express the result of these adaptations

$$P^*(fracture) = 1 - \exp\left[-\int_{V} \left(\frac{\eta - \eta_{th}}{\eta_{cr}^{SR} - \eta_{th}}\right)^m \cdot \frac{dV}{V_0}\right]$$
when $\eta \ge \eta_{th}$ (10)

$$P^*(fracture) = 0$$
 when $\eta < \eta_{th}$ (11)

where $P^*(fracture)$ = probability of fracture given the applied η -field, which may be computed at any location using Eqs. (1) and (3), and the material parameters η_{cr}^{SR} , m, and η_{th} , η_{cr}^{SR} = material toughness parameter analogous to σ_u in Eq. (5); and m = variability in the material toughness. The parameters η_{th} , η_{cr}^{SR} , and m must be selected in concert with an arbitrary reference volume V_0 , which is selected to be unity (i.e., 1 mm³) by convention (Matos and Dodds 2001). Once these three parameters are selected, the probability of fracture at any instant of loading may be readily computed by evaluating Eqs. (10) and (11), in which the integrand of Eq. (10) is evaluated over the entire component. As $m \to \infty$, the cumulative distribution function (CDF) represented by Eqs. (10) and (11) approaches a Heaviside function centered at η_{cr}^{SR} (with no dispersion),

which represents a spatially homogenous material. However, because the formulation does not admit a random value of η_{cr}^{SR} , the material is not only homogenous but also deterministic. As a result, it cannot replicate the HR material (for any values of the parameters η_{th} , η_{cr}^{SR} , and m) even in its limit as $m \to \infty$. Formulating the toughness capacity η_{cr}^{SR} as a random variable mitigates this issue. More specifically, the probability $P^*(fracture)$ may be reinterpreted to represent the probability of fracture conditional on a value of η_{cr}^{SR} , such that $P^*(fracture) = P(fracture|\eta_{cr}^{SR})$. Following this, the total probability of fracture may be expressed as

$$P(fracture) = \int_{-\infty}^{\infty} P(fracture | \eta_{cr}^{SR}) \cdot f(\eta_{cr}^{SR}) \cdot d\eta_{cr}^{SR}$$
$$= \int_{-\infty}^{\infty} P^*(fracture) \cdot f(\eta_{cr}^{SR}) \cdot d\eta_{cr}^{SR}$$
(12)

In Eq. (12) (which is an application of the law of total probability, in which the left-hand side is the marginal distribution), $f(\eta_{cr}^{SR})$ is the probability distribution function of η_{cr}^{SR} , which is assumed to be a truncated normal distribution (i.e., identical to that determined for the HR representation) and is characterized by three parameters, i.e., $\mu_{\eta_{cr}^{SR}}$, $\sigma_{\eta_{cr}^{SR}}$ and $LB_{\eta_{cr}^{SR}}$. Of these, the latter may be determined as $LB_{\eta_{cr}^{SR}} = \eta_{th}$, because it represents a lower bound on η_{cr}^{SR} . The SR representation has five parameters, i.e., $\mu_{\eta_{cr}^{SR}}, \ \sigma_{\eta_{cr}^{SR}}$ $LB_{\eta_{cr}^{SR}}$, m, and l^* (which is assumed to be deterministic). When formulated in this way, the SR material representation contains the HR material representation. Specifically, the HR representation becomes a special case of the SR representation when the parameters are chosen as follows: $m = \infty$, $\mu_{\eta_{cr}^{SR}} = \mu_{\eta_{cr}^{HR}}$, $\sigma_{\eta_{cr}^{SR}} =$ $\sigma_{\eta_{cr}^{HR}}$, and $LB_{\eta_{cr}^{SR}} = LB_{\eta_{cr}^{HR}} = \eta_{th}$. Calibration of parameters for the SR representation follows a MLE-based process similar to that described previously and illustrated schematically in Fig. 6 for the HR representation, albeit with some differences. Briefly, the process includes the following steps:

- 1. A trial parameter set including five parameters $\{\mu_{\eta^{SR}_{cr}}, \sigma_{\eta^{SR}_{cr}}, LB_{\eta^{SR}_{cr}}, m, l^*\}_{trial}$ is selected.
- 2. For each FE simulation (corresponding to a specimen), the η -field is determined at each loading deformation using Eqs. (1) and (3) and subsequently used to evaluate the probability in Eqs. (10) and (11). This results in a relationship between the loading deformation and probability of fracture, i.e., the CDF of the fracture deformation of that particular specimen i and steel type j, conditional on the assumed value of η_{cr}^{SR} , i.e., $F_{HR}^{i,j}(\Delta_{fracture}^{i,j}|\eta_{cr}^{SR})$. This process is repeated for all values of η_{cr}^{SR} for which the probability density is nonnegligible.
- 3. The marginal CDF of the fracture deformation is determined as

$$F_{HR}^{i,j}(\Delta_{fracture}^{i,j}) = \int_{LB_{\eta_{cr}^{SR}}}^{\infty} F_{HR}^{i,j}(\Delta_{fracture}^{i,j}|\eta_{cr}^{SR}) \cdot f(\eta_{cr}^{SR}) \cdot d\eta_{cr}^{SR}$$

$$\tag{13}$$

where the distribution of η_{cr}^{SR} is generated from the simulated parameters $\mu_{\eta_{cr}^{SR}}$, $\sigma_{\eta_{cr}^{SR}}$, and $LB_{\eta_{cr}^{SR}}$.

- 4. The marginal CDF generated by Eq. (13) is numerically differentiated to generate the PDF of the fracture displacement, i.e., $f_{HR}^{i,j}(\Delta_{fracture}^{i,j})$.
- 5. The PDF may be used in conjunction with experimental data to estimate the likelihood of observing the experimental response of the specimen i and steel type j, in a manner similar to that for the HR representation, i.e., $L_{HR}^{i,j} = f_{HR}^{i,j}(\Delta_{fracture, test}^{i,j})$.

6. Subsequent steps involve (1) maximization of the likelihood for each steel, using a process similar to that for the HR representation [Eq. (8)] to calibrate the optimal material parameters in Table 3; and (2) multiplication of the likelihoods corresponding to the optimal parameters for each steel type to determine L_{SR}^{total} , representing the efficacy of the entire approach, including material representation; L_{SR}^{total} is determined as 4.7×10^{40} .

An examination of Table 3 and the likelihoods yields three interesting observations. First, the net likelihood L_{SR}^{total} for the SR representation is identical to its counterpart L_{HR}^{total} for the homogenous representation. Second, for each steel, the individual likelihoods L_{SR}^{j} are equal to the corresponding likelihoods L_{HR}^{j} . Third, for each steel type, the optimal parameters for the SR representation all converge to $m = \infty$, and the other parameters are identical to those for the HR representation, i.e., $\mu_{\eta_{cr}^{SR}} = \mu_{\eta_{cr}^{HR}}$, $\sigma_{\eta_{cr}^{SR}} = \sigma_{\eta_{cr}^{HR}}$, and $LB_{\eta_{cr}^{SR}} = LB_{\eta_{cr}^{HR}} = \eta_{th}$. Because the HR representation is a special case of the SR representation, these observations suggest that this special case is the most likely. In itself, this implies that spatial randomness is absent, and the material is homogenously random. However, for each of the steel types tested by Kanvinde and Deierlein (2004) and examined in this study, all specimens were extracted from the same sample of material—either a rolled plate or a rolled beam—and showed significant variability, providing evidence of spatial heterogeneity within the larger sample. A closer analysis of the results and the underlying theory resolves this apparent contradiction. Specifically, the SR representation only represents spatial heterogeneity within the sampled volumes of the specimens considered (or, more specifically, volumes of regions that undergo plastic strain), and the results (which converge to the HR representation) indicate that the specimens are effectively homogenous over these volumes, notwithstanding the possible variability in constitutive properties, which this study did not consider. However, when considered with variability in toughness in specimens extracted from a larger volume of material, this suggests that the material is heterogeneous over larger scales. In the context of previously established frameworks for heterogeneous materials, this finding may also be interpreted to mean that the coupon-scale specimens are smaller than a true representative volume element (RVE) (Hill 1963) due to gradual, larger-scale gradients in material toughness. Yin et al. (2008) and Kanit et al. (2003) identified this problem with the RVE framework for metals and composite materials, respectively, and suggested strategies to mitigate its limitations. The next section presents a series of FE simulations of a generic component to examine implications of this observation from the standpoint of predicting fracture in structural components.

Simulation of Prototype-Scale Bending Plates with Spatially Correlated Material Properties

The preceding section, when considered along with the experimental data in Table 1, suggests that (1) spatial variability in material toughness is present in structural steel and (2) the length scales associated with this variability are larger than the size of plastically strained regions of lab-scale specimens commonly used for material calibration (i.e., those in Table 1). From the perspective of structural performance assessment, it is important to know whether the prevalent framework (i.e., the HR representation) is adequate to simulate fracture in structural components and the degree to which limitations of the HR representation compromise assessments of structural reliability. Examining this rigorously requires (1) calibration specimens extracted in a manner (e.g., from preselected locations) to systematically interrogate spatial variability and (2) validation through replicate prototype-scale

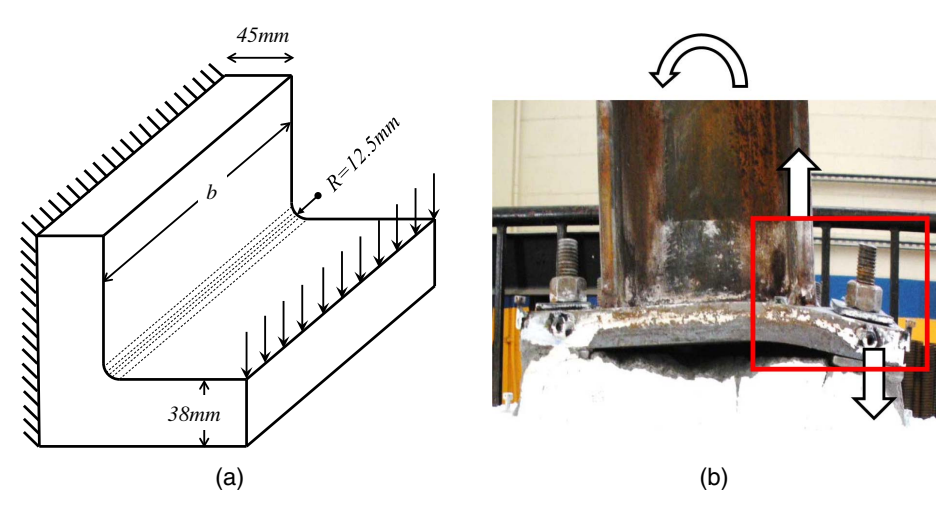


Fig. 7. Plate bending detail: (a) schematic illustration; (b) analogous region of base plate or similar structural component

experiments. Such studies have not been conducted for structural steel. In the absence of such information, FE simulations may be used to parametrically investigate the potential effect of spatial variability and randomness (and the limitations of the current approach to address it) on the fracture prediction of prototypical structural components.

To this end, this section describes a series of parametric simulations on a bending plate detail (Fig. 7). This bending plate represents a generic, fracture-critical detail (in terms of geometry, scale, and stress state) commonly found in many structural components, such as brackets, column base plates, and beam end plates, subjected to bending. Based on the previous sections, these simulations have the following characteristics: (1) although the bending plates are spatially heterogeneous when considered in their entirety, they may be considered homogenous over volumes that correspond to plastically strained regions in the test specimens described previously; and (2) the probabilistic distribution of the material toughness of these volumes is consistent with that defined for the HR representation, with its attendant parameters (i.e., $\mu_{\eta_{n}^{HR}}$, $\sigma_{\eta_{n}^{HR}}$, $LB_{\eta_{cr}^{HR}}$, and l^*) for the A572 steel (Table 3). This means that coupons, if extracted from the simulated bending plate components, would follow the statistical distribution of η_{cr} for the A572 steel as determined from actual test data (Table 1). The plate tip displacement Δ (Fig. 8) is retained as the deformation measure indicative of structural performance. Within these constraints, the FE simulations examined (1) the overall specimen scale, represented by the width of the plate b (Fig. 7); a range of values of b between 50 and 300 mm was investigated; and (2) the spatial correlation between η_{cr} at various material locations to provide a sense of the extent to which regions of clustered low-toughness may impact macroscale fracture. This study represented the spatial correlation through a semivariogram (Clark 1979)

$$Cov(h) = 1 - \gamma(h) \tag{14}$$

where

$$\gamma(h) = \frac{3h}{2\lambda} - \frac{1}{2} \left(\frac{h}{\lambda}\right)^3 \quad \text{when } h \le \lambda,$$

$$\gamma(h) = 1 \quad \text{when } h > \lambda$$
(15)

Eq. (14) provides the covariance between the η_{cr} values at any two material locations separated by a distance h. The semivariogram is a well-established concept in random field theory and

provides a rational basis for representing the internal correlation structure within a continuum, such that locations separated by large distances have uncorrelated material properties, whereas coincident material locations have identical material properties. The parameter λ is a correlation radius, such that $\lambda=\infty$ represents a perfectly homogenous material, whereas $\lambda=0$ represents a spatially stationary material (such as the SR material described previously). Consequently, λ may be interpreted as a length scale corresponding to spatial variability. This study examined values of λ in the range 5–5,000 mm.

The FE simulations themselves were qualitatively similar to those described previously in terms of meshing and constitutive models; Fig. 8 shows a representative deformed mesh. Constitutive parameters calibrated previously for the A572 steel were used to provide representation of realistic material response. The bending plate detail may be appropriately simulated through two-dimensional plane-strain FE models (Fig. 8). Similar to the previously discussed plane-strain simulations for the CT specimens,

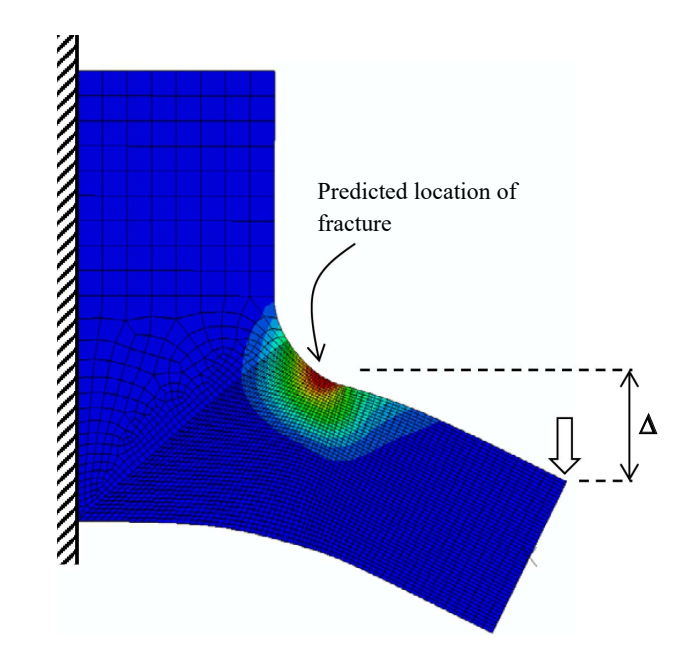


Fig. 8. Plane-strain finite-element model for bending plate detail showing contours of η

three-dimensional proxy models are regenerated from a single two-dimensional FE model by replicating the η field as determined from the plane-strain simulations through the out-of-plane dimension, representing the plate width b. As a result, the dimension b may be conveniently varied (by generating a proxy model of a different width) without running additional FE simulations. For each of the proxies (i.e., the plate widths b), material representations corresponding to each value of λ were generated. Specifically, for each λ this included the following steps:

- 1. Each proxy was discretized into cubes of dimension l_{hom} , wherein each cube may have a single value of η_{cr} . These cubes did not (in general) correspond to finite-element size, which was on the order of 0.33 mm to simulate local strain gradients. The cubes only represented regions over which the η_{cr} may be considered constant. The mapping between the constant η_{cr} and finite elements was implemented through a specially developed MATLAB script. Because the dimension l_{hom} defines the volume $V_{\text{hom}} = l_{\text{hom}}^3$ over which η_{cr} is considered constant, it may be interpreted as a discretization parameter. Convergence studies indicated that if l_{hom} was less than $\lambda/2$, the results were virtually insensitive to l_{hom} . All results in this section are for such converged values of l_{hom} .
- 2. For each such discretization, 800 realizations of a spatial field of η_{cr} (essentially representing a value of η_{cr} in each cube) were generated as part of a Monte Carlo simulation (Benjamin and Cornell 2014). Each realization represented a configuration of the η_{cr} field which was equally as likely to occur as any of the other realizations. To generate these fields, MATLAB code was developed to implement a sequential Gaussian simulation process. This process, described in detail by Goovaerts (1997), involved the following steps to develop each single realization:
 - a. Generate a random path which visits each $V_{\rm hom}$ in the domain. This may be done by numbering each $V_{\rm hom}$ and then randomizing the order in which they are visited.
 - b. For each V_{hom} along the path, a random value u may be simulated from a Gaussian distribution with mean and variance μ_G , σ_G^2 . For the first V_{hom} , the distribution is standard normal, i.e., $\mu_G = 0$, $\sigma_G^2 = 1$. For the remaining V_{hom} , the distribution is standard normal conditioned on all previously simulated u, using the correlation structure (i.e., spatial dependence) defined by Eq. (14). The conditional standard normal distribution may be expressed analytically through the mean and variance parameters (Goovaerts 1997), which are expressed in matrix form as $\mu_G = \mathbf{k}^T \cdot \mathbf{K}^{-1} \cdot \mathbf{u}$ and $\sigma_G^2 = 1 \mathbf{k}^T \cdot \mathbf{K}^{-1} \cdot \mathbf{k}$, where \mathbf{K} is a matrix containing the covariance between all

- previously simulated locations, \mathbf{k} is a vector containing the covariance between the current V_{hom} location and all previously simulated locations, and \mathbf{u} is a vector of all previously simulated values.
- c. After generating values for each V_{hom} in the domain, the standard normal variable u may be transformed to η_{cr} via the inverse CDF function, i.e., $\eta_{cr} = F^{-1}(G(u))$, where $F^{-1}(\cdot)$ is the inverse CDF of the η_{cr} distribution (Table 3) and $G(\cdot)$ is the standard Gaussian CDF.
- 3. Fig. 9 shows sample realizations of the η_{cr} field for selected values of λ ; increasing values of λ resulted in larger clusters of η_{cr} .
- 4. For each realization of the η_{cr} field, the fracture displacement $\Delta_{fracture}$ measured at the tip of the plate (Fig. 8) was determined; this was done in an identical manner as for the previously discussed (i.e., SR and HR) material representations, i.e., $\Delta_{fracture}$ was the displacement when the demand η at any location (as determined through the FE model) exceeded the capacity η_{cr} (determined through Steps 1–2) at that location.

These steps resulted in 800 values of $\Delta_{fracture}$ (one corresponding to each Monte Carlo realization of the spatial field) for each combination of b and λ . The primary objective of this section is to examine the extent to which spatial variability (over scales larger than commonly interrogated for material test coupons) may influence deformation capacities of prototype-scale structural components. Therefore Figs. 10(a and b) plot the median and standard deviation of $\Delta_{fracture}$ (as determined from the Monte Carlo simulations) against the correlation radius for three plate widths, i.e., b=50, 100, and 300 mm. The following observations may be made:

- 1. As the correlation radius λ increased, both the median and standard deviation of $\Delta_{fracture}$ increased. This was expected because a low correlation radius results in a more heterogeneous material (Fig. 9), such that the fracture deformation (which is controlled by weakest-links) is more sensitive to extreme values. As $\lambda \to \infty$, both the median and standard deviation approached that for a perfectly homogenous material whose toughness is sampled from a distribution (i.e., the HR material).
- 2. A closer examination of the curves indicates that for a given λ , the deformation capacity decreased with plate size, which is indicative of the well-known statistical size effect. Fig. 11 (discussed subsequently) addresses this in greater detail.
- 3. In addition to the trends themselves, the degree of sensitivity of $\Delta_{fracture}$ to λ was particularly notable. Specifically, for all plate

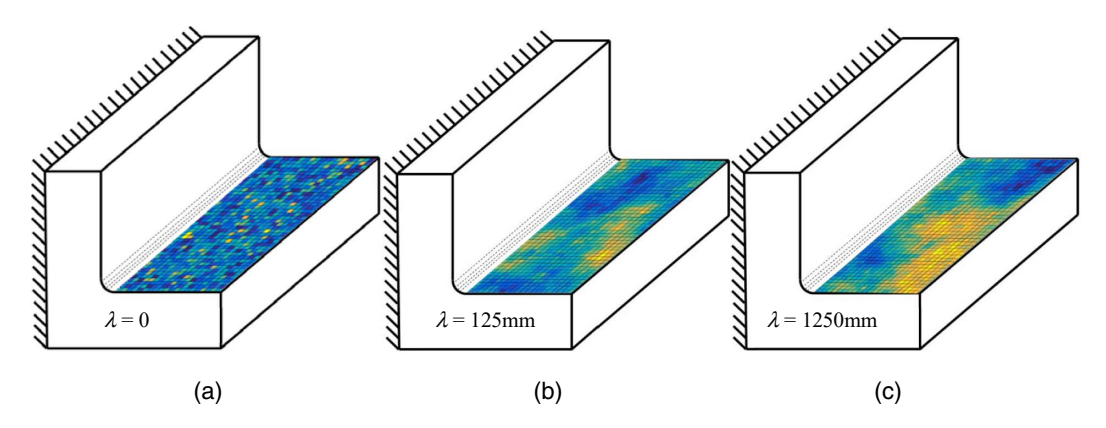


Fig. 9. Sample realizations of η_{cr} field (shown on only one surface for clarity) for three values of the correlation radius λ , showing clustering as λ increases from 0 (uncorrelated, stationary material) to 1,250 mm; $\lambda = \infty$ corresponds to homogenous material

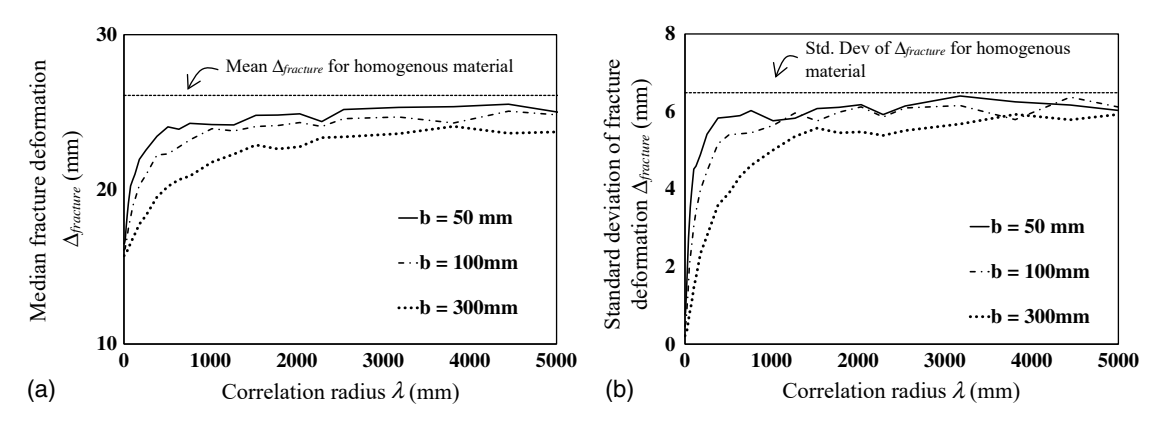


Fig. 10. Effect of correlation radius λ on predicted fracture deformation: (a) median; (b) standard deviation

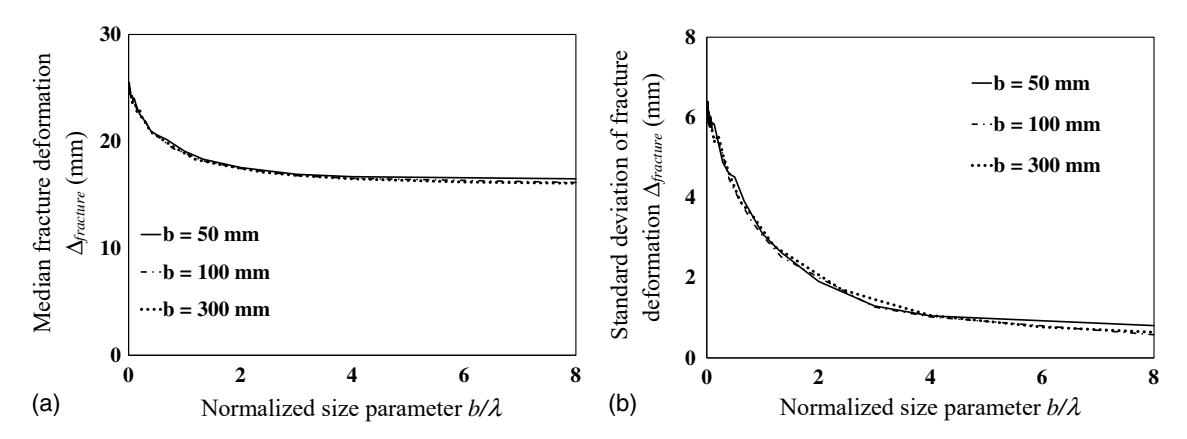


Fig. 11. Dependence of fracture deformation on normalized size b/λ : (a) median; (b) standard deviation

widths, the value of $\Delta_{fracture}$ for a $\lambda=100$ mm was approximately 25% greater than the value for $\lambda=1,000$ mm. The difference (which is controlled by the difference in the median and lower bound values of η_{cr}) diminished for larger values of λ as the curve saturated.

Point 3 is especially concerning, because all parametric simulations discussed in this section (even with widely varying values of λ) correspond to a single parent distribution of η_{cr} , which is defined by the parameters corresponding to the HR representation (Table 3). This implies that if small-scale coupons were extracted from the various material representations in Figs. 9(a-c), they would (in theory) yield an identical distribution of η_{cr} , because current methodology (Fig. 2) does not consider spatial variability or allow for determination of λ . Perhaps more importantly, in its application, the current methodology does not provide a way to distinguish between different values of λ , which, as evidenced by Fig. 10, has a strong influence on structural performance. Furthermore, $\Delta_{fracture}$ is most sensitive to λ for values of <1,000 mm λ . The test specimens (Table 1) were all extracted from rolled plates whose maximum dimension was less than 1,000 mm, indicative of significant variation over this distance, implying that λ may be well within the range in which it strongly influences structural performance. Given the sensitivity of $\Delta_{fracture}$ to λ , this further suggests that the fracture deformation of the bending plate cannot be predicted with confidence by the current methodology, which does not consider the effect of λ .

To further evaluate the size effect, Figs. 11(a and b) plot the mean and standard deviation of $\Delta_{fracture}$ against a normalized size

parameter b/λ , i.e., the width of the plate (or size) relative to the correlation radius. The curves for the various plate widths [which were separated in Figs. 10(a and b)] are virtually coincident after the normalization. This indicates that b/λ is an effective parameter for assessing the size effect, because it reconciles differences between the different plate widths. The coincident curves (which may be effectively treated as one, for the purposes of discussion) have the following characteristics:

- 1. As expected, both the mean and standard deviation of $\Delta_{fracture}$ decreased with respect to the size parameter b/λ . This is consistent with previous discussion, which noted a size-effect for larger components whose response is controlled by weakest-link processes.
- 2. The decrease in the mean and standard deviation of $\Delta_{fracture}$ was rapid for values of $<2.0b/\lambda$; for larger values of b/λ a decrease was still noted, although it was not quite as rapid. For example, for $b/\lambda = 0$ –2 the mean $\Delta_{fracture}$ decreased by 30%, whereas for $b/\lambda = 4$ –6 it decreased by 1%. This type of information is critical when transferring material parameters between components of different sizes, such as between labscale coupons and archetype-scale components. As an example, based on the trends observed in Fig. 11, it may be argued that results may be transferred with greater confidence between components with b/λ in the range 4–6, than between components with b/λ in the range 0–4.

Although the parameter b/λ appears to be quite useful, it requires the determination of the correlation radius λ . At present, there are no data for this, although the variation within specimens

extracted from samples of size <1,000 mm suggests that λ is lower than this value. This suggests that characterizing λ (or, more generally, information about spatial variability) is critical for scaling and transferring fracture toughness results between components/specimens of dissimilar size.

Summary, Conclusions, and Limitations

Despite advances in the mechanistic aspects of local models for ductile fracture in structural steel, spatial variability in toughness is commonly disregarded in the calibration and application of these models. This contradicts experimental data, which show significant variability in properties of coupons extracted from larger plates or rolled shapes. Notwithstanding this, current methodologies for applying local models assume calibration specimens and structural components to be spatially homogenous, disregarding weakest-link processes in ductile fracture. This is problematic for predicting ductile fracture initiation in large structural components based on calibration data from smaller coupon specimens. Spatial variability potentiates a statistical size effect due to weakest-link sampling, with the prospect of unconservative predictions of fracture.

Motivated by this, this study considered two competing representations of the spatial distribution of the material toughness parameter η_{cr} . One is the prevailing methodology, which assumes that the material is homogenous, i.e., η_{cr} is constant within a component or specimen. However, as is often assumed in practice, this η_{cr} itself may be random to reflect variability between replicate components; this is denoted the homogenous random representation. The other (denoted the stationary random representation) was inspired by the Weibull stress approach (Beremin 1983), which admits spatial variability within a component. The relative efficacy of these approaches was assessed through a MLE-based method. The key finding is that the SR representation does not offer a significant improvement over the HR representation in terms of reproducing test data. In fact, the parameters of the SR representation converged to those that represent an HR material, suggesting that the tested coupons may be considered homogenous over their respective volumes, although the η_{cr} varies from coupon to coupon. However, these coupons (of sizes <30 mm) were extracted from a single piece of material (~1,000 mm). Considered together, these observations suggest that variability in material toughness is present, albeit over length scales larger than coupon size. Test data that rigorously measure this type of variation are not available in the literature. Consequently, the implications of this finding were examined parametrically through FE simulations on a bending plate model that represented a generic fracture-critical detail.

The bending plate was used to examine material representations that reflect homogeneity over lengths corresponding to coupon sizes but that admit heterogeneity over larger scales (which is consistent with the implications of the HR versus SR study). Within this construct, materials were simulated as ranging from being spatially uncorrelated (i.e., a correlation radius $\lambda = 0$) to highly correlated ($\lambda = 5,000$ mm), i.e., approaching homogenous as $\lambda \to \infty$. The width of the bending plate was varied as an additional parameter. The results indicate that estimates of $\Delta_{fracture}$ varied by as much as 23% for λ values in the range 50–750 mm. This is a concerning observation because these disparate estimates were all consistent with the statistical distribution of $\eta_{\it cr}$ as obtained from test data (in accordance with current calibration procedures). Without an independent characterization of λ , it is not possible to determine which of these estimates represents true response. Additionally, a statistical size effect was observed, such that plates with greater width showed lower deformation capacity. However, the width of the plate normalized by the correlation radius, i.e., b/λ , was strongly correlated with deformation capacity, suggesting that b/λ is an effective scaling parameter for transferring test data from coupon to component scales.

The limitations of the study must be considered in its interpretation and generalization. First, the experimental data set was of a modest size, and included two types of low-carbon steel. Because spatial variability is directly linked to microstructure (e.g., inclusion distribution and grain size), extrapolation to other steel varieties requires caution. Second, weakest-link analogies are usually more appropriate for brittle fracture, because failure of the weakest link rapidly propagates to the entire component. However, in this case it is critical to note that the weakest-link analogy was not used for complete fracture of the component but rather to predict the initiation of ductile fracture only, at the first location at which such a weakest link was encountered. Although the analogy is defensible in this context, the notion of weakest-link failure may still be questioned due to the possibility of stress redistribution and deformation ductility at microstructural scales. Third, all uncertainty in the estimates was assumed to arise from randomness in the material toughness, implicitly assuming that the predictive model itself (i.e., the VGM) is unbiased and accurate—this assumption is also subject to criticism. Specifically, more-refined models have additional parameters and are able to simulate more general cases with greater accuracy. For example, Kanvinde and Deierlein (2006) addressed cyclic loading and fracture, whereas models by Bao and Wierzbicki (2004) and Benzerga et al. (2004) addressed low triaxiality and void coalescence, respectively. The higher accuracy and generality of these models is accompanied by a greater number of parameters that require calibration. In the context of this study, which focuses on randomness and spatial variability, an increase in the number of parameters triggers a highly disproportionate increase in the effort/expense of calibration because crosscorrelations and other conditional relationships must either be calibrated or assumed (the latter creating the potential for additional error). Consequently, this study selected the VGM, recognizing its limitations. Moreover, even within the VGM, only the η_{cr} is assumed to be random and heterogeneous, whereas l^* is assumed to be deterministic. The additional complexity required to calibrate the joint distributions of η_{cr} and l^* , in addition to their spatial randomness, is outside the purview of this study. In addition to the aforementioned limitations of the VGM itself, the stress and strain fields on which the VGM (or other damage mechanics models) relies are sensitive to the material constitutive parameters (i.e., yield surface and hardening laws), and to constitutive model itself (in this case, the Armstrong-Frederick model). These constitutive parameters are subject to issues similar to the fracture toughness parameters, i.e., uncertainty in estimation (e.g., Cooke and Kanvinde 2015) or spatial variability. This study did not examine the effect of these uncertainties, and their interaction with fracture toughness. As a result, it was not possible to determine what the effect of these interactions may be.

The plate bending simulations were numerical experiments on hypothetical structural details to probe the possible limitations of the prevailing framework. Without complementary experimental data (including the characterization of the correlation radius λ), these limitations cannot be confirmed. Nevertheless, the simulations pointed to the potential existence of these limitations, to motivate future research. Additionally, these simulations used a simplistic representation of the spatially correlated material, with one parameter λ . Although this is appropriate for an exploratory examination, more-sophisticated complex material structures, such as anisotropy, may require alternate representations of the spatially random field. Finally, this study focused on ductile fracture

initiation. Although this is important, it is only one process (along with ductile propagation, transition to cleavage, and brittle propagation) contributing to structural failure. Moreover, fracture initiation itself may be preceded by fatigue damage. Despite these limitations, the study provokes critical examination of flaws in the current methodology to predict ductile fracture and provides direction for future research.

References

- Amiri, H. R., Aghakouchak, A. A., Shahbeyk, S., and Engelhardt, M. D. (2013). "Finite element simulation of ultra low cycle fatigue cracking in steel structures." J. Constr. Steel Res., 89, 175–184.
- Anderson, T. L. (1995). Fracture mechanics, 2nd Ed., CRC Press, Boca Raton, FL.
- Andrade, J. E., Baker, J. W., and Ellison, K. C. (2008). "Random porosity fields and their influence on the stability of granular media." *Int. J. Numer. Anal. Methods Geomech.*, 32(10), 1147–1172.
- Armstrong, P. J., and Frederick, C. O. (1966). "A mathematical representation of the multiaxial Bauschinger effect." Berkeley Nuclear Laboratories, Research and Development Dept., Berkeley, CA.
- ASTM. (2013). "Standard test method for measurement of fracture toughness." ASTM E1820, West Conshohocken, PA.
- Bao, Y., and Wierzbicki, T. (2004). "On fracture locus in the equivalent strain and stress triaxiality space." *Int. J. Mech. Sci.*, 46(1), 81–98.
- Bažant, Z. P. (2005). Scaling of structural strength, 2nd Ed., Butterworth-Heineman, Oxford, U.K.
- Bažant, Z. P., Pang, S. D., Vořechovský, M., Novak, D., and Pukl, R. (2004). "Statistical size effect in quasibrittle materials: Computation and extreme value theory." Proc., FraMCoS-5, 5th Int. Conf. on Fracture Mechanics of Concrete and Concrete Structures, V. C. Li, K. Y. Leung, K. J. Willam, and S. L. Billington, eds., Vol. 1, IA-FraMCoS, Vail, CO, 189–196.
- Becker, R. (1987). "The effect of porosity distribution on ductile failure." J. Mech. Phys. Solids, 35(5), 577–599.
- Benjamin, J. R., and Cornell, C. A. (2014). *Probability, statistics, and decision for civil engineers*, Dover Books on Engineering, Mineola, NY.
- Benzerga, A., Besson, J., and Pineau, A. (2004). "Anisotropic ductile fracture. Part II: Theory." *Acta Mater.*, 52(15), 4639–4650.
- Beremin, F. M. (1983). "A local criterion for cleavage fracture of a nuclear pressure vessel steel." *Metall. Trans. A*, 14(11), 2277–2287.
- Besson, J., Moinereau, D., and Steglich, D. (2006). "Local approach to fracture." 9th European Mechanics of Materials Conference Euromech-Mecamat, European Mechanics Society, Moret-sur-Loing, France.
- Chen, Z., and Butler, C. (2013). Micromechanics of modeling ductile fracture, solid mechanics and its applications, Springer, New York.
- Chi, W. M., Deierlein, G., and Ingraffea, A. (2000). "Fracture toughness demands in welded beam-column moment connections." *J. Struct. Eng.*, 10.1061/(ASCE)0733-9445(2000)126:1(88), 88–97.
- Chi, W. M., Kanvinde, A. M., and Deierlein, G. (2006). "Prediction of ductile fracture in welded connections using the SMCS criterion." *J. Struct. Eng.*, 10.1061/(ASCE)0733-9445(2006)132:2(171), 171–181.
- Clark, I. (1979). Practical geostatistics, Applied Science, London.
- Cooke, R. J., and Kanvinde, A. M. (2015). "Constitutive parameter calibration for structural steel: Non-uniqueness and loss of accuracy." J. Constr. Steel Res., 114, 394–404.
- de Geus, T. W. J., Peerlings, R. H. J., and Geers, M. G. D. (2015). "Microstructural modeling of ductile fracture initiation in multiphase materials." *Eng. Fract. Mech.*, 147, 318–330.
- Devillers-Guerville, L., Besson, J., and Pineau, A. (1997). "Notch fracture toughness of a cast duplex stainless steel; modelling of experimental scatter and size effect." *Nucl. Eng. Des.*, 168(1–3), 211–225.
- FEMA. (2000). "Recommended design criteria for new steel moment-frame buildings." *FEMA-350*, Washington, DC.
- FEMA. (2009). "Quantification of building seismic performance factors." *FEMA-P695*, Washington, DC.
- Feng, X., Lu, Z. X., Yang, Z. Y., and Guo, J. H. (2011). "Analysis on the variances of material and structural properties based on random field theory." *Probab. Eng. Mech.*, 26(2), 222–230.

- Gao, X., Ruggieri, C., and Dodds, R. H., Jr. (1998). "Calibration of Weibull stress models using fracture toughness data." *Int. J. Fract.*, 92(2), 175–200.
- Goovaerts, P. (1997). Geostatistics for natural resources evaluation, Oxford University Press, New York.
- Gurson, A. L. (1977). "Continuum theory of ductile rupture by void nucleation and growth. Part I: Yield criteria and flow rules for porous ductile media." J. Eng. Mater. Technol., 99, 2–15.
- Hampel, F. R., Ronchetti, E. M., Rousseeuw, P. J., and Stahel, W. A. (1986). Robust statistics, Wiley, New York.
- Hancock, J. W., and Mackenzie, A. C. (1976). "On the mechanics of ductile failure in high-strength steel subjected to multi-axial stress-states." *J. Mech. Phys. Solids*, 24(2–3), 147–160.
- Hazarabedian, A., Forget, P., and Bernard, M. (2002). "Local approach to fracture of an aged duplex stainless steel." *Mater. Res.*, 5(2), 131–135.
- Hill, R. (1963). "Elastic properties of reinforced solids: Some theoretical principles." J. Mech. Phys. Solids, 11, 357–372.
- Hoel, P. G. (1962). Introduction to mathematical statistics, 3rd Ed., Wiley, New York.
- Jeulin, D., and Ostoja-Starzewski, M. (2001). Mechanics of random multiscale microstructures, Springer, Berlin.
- Kanit, T., Forest, S., Galliet, I., Mounoury, V., and Jeulin, D. (2003). "Determination of the size of the representative volume element for random composites: Statistical and numerical approach." *Int. J. Solids* Struct., 40(13–14), 3647–3679.
- Kanvinde, A. M. (2017). "Predicting fracture in civil engineering steel structures: State of the art." J. Struct. Eng., 10.1061/(ASCE)ST.1943 -541X.0001704, 03116001.
- Kanvinde, A. M., and Deierlein, G. G. (2004). "Micromechanical simulation of earthquake induced fracture in steel structures." *Technical Rep. 145*, John A. Blume Earthquake Engineering Center, Stanford Univ., Stanford, CA.
- Kanvinde, A. M., and Deierlein, G. G. (2006). "The void growth model and the stress modified critical strain model to predict ductile fracture in structural steels." J. Struct. Eng., 10.1061/(ASCE)0733-9445(2006) 132:12(1907), 1907–1918.
- Kanvinde, A. M., and Deierlein, G. G. (2007). "A cyclic void growth model to assess ductile fracture in structural steels due to ultra low cycle fatigue." J. Eng. Mech., 10.1061/(ASCE)0733-9399(2007)133:6(701), 701–712.
- Khandelwal, K., and El-Tawil, S. (2007). "Collapse behavior of steel special moment resisting frame connections." *J. Struct. Eng.*, 10.1061 /(ASCE)0733-9445(2007)133:5(646), 646–655.
- Kiran, R., and Khandelwal, K. (2013). "Experimental studies and models for ductile fracture in ASTM A992 steels at high triaxiality." J. Struct. Eng., 10.1061/(ASCE)ST.1943-541X.0000828, 04013044.
- Lambert-Perlade, A., Sturel, T., Gourgues, A. F., Besson, J., and Pineau, A. (2004). "Mechanisms and modeling of cleavage fracture in simulated heat-affected zone microstructures of a high-strength low alloy steel." Metall. Mater. Trans. A, 35(3), 1039–1053.
- Liao, F., Wang, W., and Chen, Y. (2012). "Parameter calibrations and application of micromechanical fracture models of structural steels." *Struct. Eng. Mech.*, 42(2), 153–174.
- MATLAB version 9.0 [Computer software]. MathWorks, Inc., Natick, MA. Matos, C. G., and Dodds, R. H. (2001). "Probabilistic modelling of weld fracture in steel frame connections. Part I: Quasi-static loading." Eng. Struct., 23(8), 1011–1030.
- McClintock, F. A. (1968). "A criterion for ductile fracture by the growth of holes." *J. Appl. Mech.*, 35(2), 363–371.
- Myers, A. T., Deierlein, G. G., and Kanvinde, A. M. (2009). "Testing and probabilistic simulation of ductile fracture initiation in structural steel components and weldments." *Technical Rep. 170*, John A. Blume Earthquake Engineering Center, Stanford Univ., Stanford, CA.
- Myers, A. T., Kanvinde, A. M., and Deierlein, G. G. (2010). "Calibration of the stress modified critical strain (SMCS) criterion to predict fracture in structural details: Specimen size dependence and parameter assessment." J. Eng. Mech., 10.1061/(ASCE)EM.1943-7889.0000178, 1401–1410.
- Myers, A. T., Kanvinde, A. M., Deierlein, G. G., and Baker, J. W. (2014). "A probabilistic formulation of the cyclic void growth model to predict

- ultra low cycle fatigue in structural steel." *J. Eng. Mech.*, 10.1061 /(ASCE)EM.1943-7889.0000728, 0401402.
- Panontin, T. L., and Sheppard, S. D. (1995). "The relationship between constraint and ductile fracture initiation as defined by micromechanical analyses." Fracture Mechanics: 26th Volume, ASTM, Reston, VA, 1256.
- Paquet, D., and Ghosh, S. (2011). "Microstructural effects on ductile fracture in heterogeneous materials. Part I: Sensitivity analysis with LE-VCFEM." Eng. Fract. Mech., 78(2), 205–225.
- Pineau, A., and Joly, P. (1991). "Local versus global approaches to elastic-plastic fracture mechanics." *Defect assessment in components— Fundamentals and applications*, J. G. Blauel and K. H. Schwalbe, eds., Mechanical Engineering Publications, London, 381–414.
- Ponson, L., Cao, Y., Bouchaud, E., Tvergaard, V., and Needleman, A. (2013). "Statistics of ductile fracture surfaces: The effect of material parameters." *Int. J. Fract.*, 184(1–2), 137–149.
- Prinz, G. S., and Richards, P. W. (2015). "Demands on reduced beam section connections with out-of-plane skew." J. Struct. Eng., 10.1061 /(ASCE)ST.1943-541X.0001360, 04015095.
- Rice, J. R., and Tracey, D. M. (1969). "On the ductile enlargement of voids in triaxial stress fields." J. Mech. Phys. Solids, 17(3), 201–217.

- Ritchie, R. O., Knott, J. F., and Rice, J. R. (1973). "On the relationship between critical tensile stress and fracture toughness in mild steel." *J. Mech. Phys. Solids*, 21(6), 395–410.
- Smith, C. M., Deierlein, G. G., and Kanvinde, A. M. (2014). "A stress-weighted damage model for ductile fracture initiation in structural steel under cyclic loading and generalized stress states." TR 187, Blume Earthquake Engineering Center, Stanford Univ., Stanford, CA.
- Smith, C. M., Kanvinde, A. M., and Deierlein, G. G. (2017). "Calibration of continuum cyclic constitutive models for structural steel using particle swarm optimization." *J. Eng. Mech.*, 10.1061/(ASCE)EM.1943-7889 .0001214, 04017012.
- Weibull, W. (1939). "The phenomenon of rupture in solids." *Proc., Royal Swedish Institute of Engineering Research*, The Royal Swedish Academy of Engineering Sciences, Stockholm, Sweden, 1–55.
- Wen, H., and Mahmoud, H. (2016). "New model for ductile fracture of metal alloys. I: Monotonic loading." J. Eng. Mech., 10.1061/(ASCE) EM.1943-7889.0001009, 04015088.
- Yin, X., Chen, W., To, A., McVeigh, C., and Liu, W. K. (2008). "Statistical volume element method for predicting microstructure-constitutive property relations." *Comput. Methods Appl. Mech. Eng.*, 197(43–44), 3516–3529.